DESY 01–093
June 2001
ISSN 0418-9833

Measurement of Deeply Virtual Compton Scattering at HERA

H1 Collaboration

Abstract

A measurement is presented of elastic Deeply Virtual Compton Scattering $e^+ + p \to e^+ + \gamma + p$ at HERA using data taken with the H1 detector. The cross section is measured as a function of the photon virtuality, Q^2, and the invariant mass, W, of the γp system, in the kinematic range $2 < Q^2 < 20\,\mathrm{GeV}^2$, $30 < W < 120\,\mathrm{GeV}$ and $|t| < 1\,\mathrm{GeV}^2$, where t is the squared momentum transfer to the proton. The measurement is compared to QCD based calculations.

To be submitted to Physics Letters B

C. Adloff[33], V. Andreev[24], B. Andrieu[27], T. Anthonis[4], V. Arkadov[35], A. Astvatsatourov[35], A. Babaev[23], J. Bähr[35], P. Baranov[24], E. Barrelet[28], W. Bartel[10], P. Bate[21], A. Beglarian[34], O. Behnke[13], C. Beier[14], A. Belousov[24], T. Benisch[10], Ch. Berger[1], T. Berndt[14], J.C. Bizot[26], V. Boudry[27], W. Braunschweig[1], V. Brisson[26], H.-B. Bröker[2], D.P. Brown[10], W. Brückner[12], D. Bruncko[16], J. Bürger[10], F.W. Büsser[11], A. Bunyatyan[12,34], A. Burrage[18], G. Buschhorn[25], L. Bystritskaya[23], A.J. Campbell[10], J. Cao[26], S. Caron[1], D. Clarke[5], B. Clerbaux[4], C. Collard[4], J.G. Contreras[7,41], Y.R. Coppens[3], J.A. Coughlan[5], M.-C. Cousinou[22], B.E. Cox[21], G. Cozzika[9], J. Cvach[29], J.B. Dainton[18], W.D. Dau[15], K. Daum[33,39], M. Davidsson[20], B. Delcourt[26], N. Delerue[22], R. Demirchyan[34], A. De Roeck[10,43], E.A. De Wolf[4], C. Diaconu[22], J. Dingfelder[13], P. Dixon[19], V. Dodonov[12], J.D. Dowell[3], A. Droutskoi[23], A. Dubak[25], C. Duprel[2], G. Eckerlin[10], D. Eckstein[35], V. Efremenko[23], S. Egli[32], R. Eichler[36], F. Eisele[13], E. Eisenhandler[19], M. Ellerbrock[13], E. Elsen[10], M. Erdmann[10,40,e], W. Erdmann[36], P.J.W. Faulkner[3], L. Favart[4], A. Fedotov[23], R. Felst[10], J. Ferencei[10], S. Ferron[27], M. Fleischer[10], Y.H. Fleming[3], G. Flügge[2], A. Fomenko[24], I. Foresti[37], J. Formánek[30], J.M. Foster[21], G. Franke[10], E. Gabathuler[18], K. Gabathuler[32], J. Garvey[3], J. Gassner[32], J. Gayler[10], R. Gerhards[10], C. Gerlich[13], S. Ghazaryan[4,34], L. Goerlich[6], N. Gogitidze[24], M. Goldberg[28], C. Goodwin[3], C. Grab[36], H. Grässler[2], T. Greenshaw[18], G. Grindhammer[25], T. Hadig[13], D. Haidt[10], L. Hajduk[6], W.J. Haynes[5], B. Heinemann[18], G. Heinzelmann[11], R.C.W. Henderson[17], S. Hengstmann[37], H. Henschel[35], R. Heremans[4], G. Herrera[7,44], I. Herynek[29], M. Hildebrandt[37], M. Hilgers[36], K.H. Hiller[35], J. Hladký[29], P. Höting[2], D. Hoffmann[22], R. Horisberger[32], S. Hurling[10], M. Ibbotson[21], Ç. İşsever[7], M. Jacquet[26], M. Jaffre[26], L. Janauschek[25], X. Janssen[4], V. Jemanov[11], L. Jönsson[20], D.P. Johnson[4], M.A.S. Jones[18], H. Jung[20,10], H.K. Kästli[36], D. Kant[19], M. Kapichine[8], M. Karlsson[20], O. Karschnick[11], F. Keil[14], N. Keller[37], J. Kennedy[18], I.R. Kenyon[3], S. Kermiche[22], C. Kiesling[25], P. Kjellberg[20], M. Klein[35], C. Kleinwort[10], T. Kluge[1], G. Knies[10], B. Koblitz[25], S.D. Kolya[21], V. Korbel[10], P. Kostka[35], S.K. Kotelnikov[24], R. Koutouev[12], A. Koutov[8], H. Krehbiel[10], J. Kroseberg[37], K. Krüger[10], A. Küpper[33], T. Kuhr[11], T. Kurča[25,16], R. Lahmann[10], D. Lamb[3], M.P.J. Landon[19], W. Lange[35], T. Laštovička[35], P. Laycock[18], E. Lebailly[26], A. Lebedev[24], B. Leißner[1], R. Lemrani[10], V. Lendermann[7], S. Levonian[10], M. Lindstroem[20], B. List[36], E. Lobodzinska[10,6], B. Lobodzinski[6,10], A. Loginov[23], N. Loktionova[24], V. Lubimov[23], S. Lüders[36], D. Lüke[7,10], L. Lytkin[12], H. Mahlke-Krüger[10], N. Malden[21], E. Malinovski[24], I. Malinovski[24], R. Maraček[25], P. Marage[4], J. Marks[13], R. Marshall[21], H.-U. Martyn[1], J. Martyniak[6], S.J. Maxfield[18], D. Meer[36], A. Mehta[18], K. Meier[14], A.B. Meyer[11], H. Meyer[33], J. Meyer[10], P.-O. Meyer[2], S. Mikocki[6], D. Milstead[18], T. Mkrtchyan[34], R. Mohr[25], S. Mohrdieck[11], M.N. Mondragon[7], F. Moreau[27], A. Morozov[8], J.V. Morris[5], K. Müller[37], P. Murín[16,42], V. Nagovizin[23], B. Naroska[11], J. Naumann[7], Th. Naumann[35], G. Nellen[25], P.R. Newman[3], T.C. Nicholls[5], F. Niebergall[11], C. Niebuhr[10], O. Nix[14], G. Nowak[6], J.E. Olsson[10], D. Ozerov[23], V. Panassik[8], C. Pascaud[26], G.D. Patel[18], M. Peez[22], E. Perez[9], J.P. Phillips[18], D. Pitzl[10], R. Pöschl[26], I. Potachnikova[12], B. Povh[12], K. Rabbertz[1], G. Rädel[27], J. Rauschenberger[11], P. Reimer[29], B. Reisert[25], D. Reyna[10], C. Risler[25], E. Rizvi[3], P. Robmann[37], R. Roosen[4], A. Rostovtsev[23], S. Rusakov[24], K. Rybicki[6], D.P.C. Sankey[5], J. Scheins[1], F.-P. Schilling[10], P. Schleper[10], D. Schmidt[33], D. Schmidt[10], S. Schmidt[25], S. Schmitt[10], M. Schneider[22], L. Schoeffel[9], A. Schöning[36], T. Schörner[25], V. Schröder[10], H.-C. Schultz-Coulon[7], C. Schwanenberger[10], K. Sedlák[29], F. Sefkow[37], V. Shekelyan[25], I. Sheviakov[24], L.N. Shtarkov[24], Y. Sirois[27], T. Sloan[17], P. Smirnov[24], Y. Soloviev[24], D. South[21], V. Spaskov[8], A. Specka[27], H. Spitzer[11], R. Stamen[7], B. Stella[31],

J. Stiewe[14], U. Straumann[37], M. Swart[14], M. Taševský[29], V. Tchernyshov[23], S. Tchetchelnitski[23], G. Thompson[19], P.D. Thompson[3], N. Tobien[10], D. Traynor[19], P. Truöl[37], G. Tsipolitis[10,38], I. Tsurin[35], J. Turnau[6], J.E. Turney[19], E. Tzamariudaki[25], S. Udluft[25], M. Urban[37], A. Usik[24], S. Valkár[30], A. Valkárová[30], C. Vallée[22], P. Van Mechelen[4], S. Vassiliev[8], Y. Vazdik[24], A. Vichnevski[8], K. Wacker[7], R. Wallny[37], B. Waugh[21], G. Weber[11], M. Weber[14], D. Wegener[7], C. Werner[13], M. Werner[13], N. Werner[37], G. White[17], S. Wiesand[33], T. Wilksen[10], M. Winde[35], G.-G. Winter[10], Ch. Wissing[7], M. Wobisch[10], E. Wünsch[10], A.C. Wyatt[21], J. Žáček[30], J. Zálešák[30], Z. Zhang[26], A. Zhokin[23], F. Zomer[26], J. Zsembery[9], and M. zur Nedden[10]

[1] *I. Physikalisches Institut der RWTH, Aachen, Germany*[a]
[2] *III. Physikalisches Institut der RWTH, Aachen, Germany*[a]
[3] *School of Physics and Space Research, University of Birmingham, Birmingham, UK*[b]
[4] *Inter-University Institute for High Energies ULB-VUB, Brussels; Universitaire Instelling Antwerpen, Wilrijk; Belgium*[c]
[5] *Rutherford Appleton Laboratory, Chilton, Didcot, UK*[b]
[6] *Institute for Nuclear Physics, Cracow, Poland*[d]
[7] *Institut für Physik, Universität Dortmund, Dortmund, Germany*[a]
[8] *Joint Institute for Nuclear Research, Dubna, Russia*
[9] *CEA, DSM/DAPNIA, CE-Saclay, Gif-sur-Yvette, France*
[10] *DESY, Hamburg, Germany*
[11] *II. Institut für Experimentalphysik, Universität Hamburg, Hamburg, Germany*[a]
[12] *Max-Planck-Institut für Kernphysik, Heidelberg, Germany*[a]
[13] *Physikalisches Institut, Universität Heidelberg, Heidelberg, Germany*[a]
[14] *Kirchhoff-Institut für Physik, Universität Heidelberg, Heidelberg, Germany*[a]
[15] *Institut für experimentelle und Angewandte Physik, Universität Kiel, Kiel, Germany*[a]
[16] *Institute of Experimental Physics, Slovak Academy of Sciences, Košice, Slovak Republic*[e,f]
[17] *School of Physics and Chemistry, University of Lancaster, Lancaster, UK*[b]
[18] *Department of Physics, University of Liverpool, Liverpool, UK*[b]
[19] *Queen Mary and Westfield College, London, UK*[b]
[20] *Physics Department, University of Lund, Lund, Sweden*[g]
[21] *Physics Department, University of Manchester, Manchester, UK*[b]
[22] *CPPM, CNRS/IN2P3 - Univ Mediterranee, Marseille - France*
[23] *Institute for Theoretical and Experimental Physics, Moscow, Russia*[l]
[24] *Lebedev Physical Institute, Moscow, Russia*[e,h]
[25] *Max-Planck-Institut für Physik, München, Germany*[a]
[26] *LAL, Université de Paris-Sud, IN2P3-CNRS, Orsay, France*
[27] *LPNHE, Ecole Polytechnique, IN2P3-CNRS, Palaiseau, France*
[28] *LPNHE, Universités Paris VI and VII, IN2P3-CNRS, Paris, France*
[29] *Institute of Physics, Academy of Sciences of the Czech Republic, Praha, Czech Republic*[e,i]
[30] *Faculty of Mathematics and Physics, Charles University, Praha, Czech Republic*[e,i]
[31] *Dipartimento di Fisica Università di Roma Tre and INFN Roma 3, Roma, Italy*
[32] *Paul Scherrer Institut, Villigen, Switzerland*
[33] *Fachbereich Physik, Bergische Universität Gesamthochschule Wuppertal, Wuppertal, Germany*[a]
[34] *Yerevan Physics Institute, Yerevan, Armenia*

[35] *DESY, Zeuthen, Germany*[a]
[36] *Institut für Teilchenphysik, ETH, Zürich, Switzerland*[j]
[37] *Physik-Institut der Universität Zürich, Zürich, Switzerland*[j]
[38] *Also at Physics Department, National Technical University, Zografou Campus, GR-15773 Athens, Greece*
[39] *Also at Rechenzentrum, Bergische Universität Gesamthochschule Wuppertal, Germany*
[40] *Also at Institut für Experimentelle Kernphysik, Universität Karlsruhe, Karlsruhe, Germany*
[41] *Also at Dept. Fis. Ap. CINVESTAV, Mérida, Yucatán, México*[k]
[42] *Also at University of P.J. Šafárik, Košice, Slovak Republic*
[43] *Also at CERN, Geneva, Switzerland*
[44] *Also at Dept. Fis. CINVESTAV, México City, México*[k]

[a] *Supported by the Bundesministerium für Bildung, Wissenschaft, Forschung und Technologie, FRG, under contract numbers 7AC17P, 7AC47P, 7DO55P, 7HH17I, 7HH27P, 7HD17P, 7HD27P, 7KI17I, 6MP17I and 7WT87P*
[b] *Supported by the UK Particle Physics and Astronomy Research Council, and formerly by the UK Science and Engineering Research Council*
[c] *Supported by FNRS-NFWO, IISN-IIKW*
[d] *Partially Supported by the Polish State Committee for Scientific Research, grant no. 2P0310318 and SPUB/DESY/P03/DZ-1/99, and by the German Federal Ministry of Education and Science, Research and Technology (BMBF)*
[e] *Supported by the Deutsche Forschungsgemeinschaft*
[f] *Supported by VEGA SR grant no. 2/5167/98*
[g] *Supported by the Swedish Natural Science Research Council*
[h] *Supported by Russian Foundation for Basic Research grant no. 96-02-00019*
[i] *Supported by the Ministry of Education of the Czech Republic under the projects INGO-LA116/2000 and LN00A006, and by GA AVČR grant no B1010005*
[j] *Supported by the Swiss National Science Foundation*
[k] *Supported by CONACyT*
[l] *Partially Supported by Russian Foundation for Basic Research, grant no. 00-15-96584*

1 Introduction

This paper presents the first measurement of the elastic cross section for Deeply Virtual Compton Scattering (DVCS) (Fig. 1a) i.e. the diffractive scattering of a virtual photon off a proton [1–6] by studying the reaction:

$$e^+ + p \rightarrow e^+ + \gamma + p. \tag{1}$$

The interest of this process, because of its apparent simplicity, resides in the particular insight it gives for the applicability of perturbative Quantum Chromo Dynamics (QCD) in the field of diffractive interactions. The wide kinematic range in the photon virtuality, Q^2, accessible at HERA, provides a powerful probe for the interplay between perturbative and non-perturbative regimes in QCD. Furthermore the DVCS process gives access to a new class of parton distribution functions, the skewed parton distributions (SPD) [7–9] which are generalisations of the familiar parton distributions and include parton momentum correlations.

The reaction studied receives contributions from both the DVCS process whose origin lies in the strong interaction, and the purely electromagnetic Bethe-Heitler (BH) process (Fig. 1b and c) where the photon is emitted from the positron line. The BH process is precisely known as it depends only on QED calculations and proton elastic form factors. The DVCS cross section is extracted by subtracting the BH contribution from the total cross section, which is possible since the interference contribution vanishes when averaged over the full azimuthal angle of the final state particles. A recent measurement of the single spin asymmetry in a longitudinally polarised electron beam [10] complements this measurement.

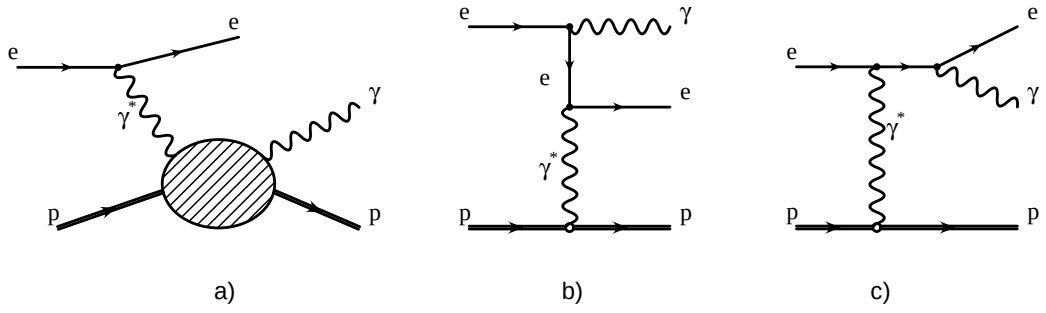

Figure 1: *The DVCS (a) and the Bethe-Heitler (b and c) processes.*

The QCD interpretation of DVCS is based on the two diagrams shown in Fig. 2. In the presence of a hard scale, the DVCS scattering amplitude factorises [2,3,9] into a hard scattering part calculable in perturbative QCD and parton distributions which contain the non-perturbative effects due to the proton structure. The DVCS process is similar to diffractive vector meson electro-production, a real photon replacing the final state vector meson. Recent measurements of diffractive vector meson production at HERA [11–15] indicate that Q^2 is relevant for the hard scale of the interaction in QCD calculation. In comparison to vector meson production, DVCS avoids the theoretical complications and uncertainties associated with the unknown vector meson wave function. However, even at Q^2 values above a few GeV^2, non perturbative effects

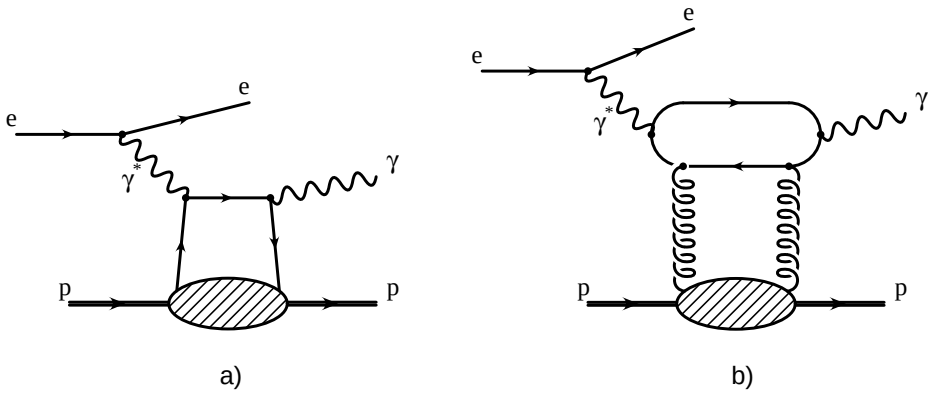

Figure 2: *The two leading DVCS diagrams in a QCD picture.*

influence the predictions and have to be modeled. The DVCS cross section is suppressed relative to that of vector meson production by the additional electromagnetic coupling.

Calculations of the DVCS cross section have been published by Frankfurt, Freund and Strikman (FFS) [16] and by Donnachie and Dosch (DD) [17]. Both contain "soft" (non-perturbative) and "hard" contributions. The soft part in the FFS prediction is based on the aligned jet model [18], whereas reggeon and soft pomeron exchanges are considered in the DD prediction. The hard contribution in FFS is calculated in perturbative QCD. The hard contribution in DD is based on a dipole model where all parameters are determined from pp and $\gamma^* p$ cross section measurements. These predictions only provide the scattering amplitude at $t = t_{min} \simeq -m_p^2 Q^4/W^4$, where $|t|$ is the squared momentum transfer to the proton, m_p the proton mass and W the invariant mass of the $\gamma^* p$ system. In both cases an exponential t-dependence, $e^{-b|t|}$, is assumed.

For the DVCS process as well as for the vector meson production, the transition from a virtual photon to an on shell particle forces the fractional momenta of the two partons involved to be unequal and imposes a correlation. Therefore, the cross section calculation necessitates the use of skewed parton distributions [7–9]. The difference in fractional momenta, the skewedness, becomes important at high Q^2 values or high vector meson masses. In particular SPDs have been introduced in order to reconcile QCD calculations with the Υ diffractive photo-production measurements at HERA [19, 20]. For vector meson production SPDs appear quadratically in the cross section expression. A unique feature of DVCS is that they appear linearly in the interference term with the Bethe-Heitler process. Therefore the DVCS measurement, in contrast to vector meson production, offers a particularly suitable channel to extract skewed parton distributions [16, 21–23].

In this paper, the elastic DVCS cross section measurement at HERA is presented differentially in Q^2 and W in the Q^2 range from 2 to $20\,\mathrm{GeV}^2$, W from 30 to $120\,\mathrm{GeV}$ and $|t|$ below $1\,\mathrm{GeV}^2$.

2 H1 Detector, Kinematics and Monte Carlo Simulation

A detailed description of the H1 detector can be found in [24]. Here only the detector components relevant for the present analysis are shortly described. The SPACAL [25], a lead – scintillating fibre calorimeter covers the backward[1] region of the H1 detector ($153^\circ < \theta < 177.5^\circ$). Its energy resolution for electromagnetic showers is $\sigma(E)/E \simeq 7.1\%/\sqrt{E/GeV} \oplus 1\%$. The uncertainty on the alignment of the calorimeter corresponds to an uncertainty of 1.3 mrad on the scattered positron polar angle. The liquid argon (LAr) calorimeter ($4^\circ \leq \theta \leq 154^\circ$) is situated inside a solenoidal magnet. The energy resolution for electromagnetic showers is $\sigma(E)/E \simeq 11\%/\sqrt{E/GeV}$ as obtained from test beam measurements [26]. The major components of the central tracking detector are two 2 m long coaxial cylindrical drift chambers, the CJC, with wires parallel to the beam direction. The measurement of charged particle transverse momenta is performed in a magnetic field of 1.15 T, uniform over the full tracker volume. The forward components of the detector, used here to tag hadronic activity at high pseudo-rapidity ($5 \lesssim \eta \lesssim 7$), are the forward muon spectrometer (FMD) and the proton remnant tagger (PRT). The FMD, designed to identify and measure the momentum of muons emitted in the forward direction, contains six active layers, each made of a pair of planes of drift cells. The three layers between the main calorimeter and the toroidal magnet can be reached by secondary particles arising from the interaction of particles scattered under small angles hitting the beam collimators or the beam pipe walls. Secondary particles or the scattered proton at large $|t|$ can also be detected by the PRT, located at 24 m from the interaction point and consisting of double layers of scintillator surrounding the beam pipe. The trigger used is based on the detection of a cluster in the electromagnetic section of the SpaCal calorimeter with an energy greater than 6 GeV.

The data were obtained with the H1 detector in the 1997 running period when the HERA collider was operated with 820 GeV protons and 27.5 GeV positrons. The sample corresponds to an integrated luminosity of $8\,\mathrm{pb}^{-1}$.

The reconstruction method for the kinematic variables Q^2 and x-Bjorken relies on the polar angle measurements of the final state electron, θ_e, and photon, θ_γ, (double angle method):

$$Q^2 = 4E_0^2 \frac{\sin\,\theta_\gamma\,(1+\cos\theta_e)}{\sin\,\theta_\gamma\,+\sin\,\theta_e\,-\sin\,(\theta_e\,+\theta_\gamma)} \tag{2}$$

$$x = \frac{E_0}{E_p}\frac{\sin\,\theta_\gamma\,+\sin\,\theta_e\,+\sin\,(\theta_e\,+\theta_\gamma)}{\sin\,\theta_\gamma\,+\sin\,\theta_e\,-\sin\,(\theta_e\,+\theta_\gamma)} \tag{3}$$

$$W^2 = \frac{Q^2}{x}\,(1-x) \tag{4}$$

where E_0 and E_p are the electron and the proton beam energies, respectively. In case a vertex cannot be reconstructed, the nominal position of the ep interactions is taken. The variable t, the square of the four-momentum transfer to the proton, is very well approximated by the negative square of the transverse momentum of the outgoing proton. The latter is computed as the vector sum of the transverse momenta of the final state photon $\vec{p}_{t_\gamma}$ and of the scattered positron $\vec{p}_{t_e}$:

$$t \simeq -|\vec{p}_{t_\gamma} + \vec{p}_{t_e}|^2\ . \tag{5}$$

[1] H1 uses a right-handed coordinate system with the z axis taken along the beam direction, the $+z$ or "forward" direction being that of the outgoing proton beam, the "transverse" directions are perpendicular to the z axis. The polar angle θ is defined with respect to the z axis. The pseudo-rapidity is defined by $\eta = -\ln\tan\theta/2$.

Monte Carlo simulations are used to estimate the corrections to be applied to the data for the acceptance and resolutions of the detector. The generated events are passed through a detailed simulation of the H1 detector and are subject to the same reconstruction and analysis chain as the data. The DVCS process is simulated (for more details see [27]) according to the predicted cross section of FFS [16], which includes the DVCS process, the Bethe-Heitler process and their interference[2]. Photon radiation from the incoming positron has been included in the simulation in the collinear approximation. The Monte Carlo generator COMPTON 2.0 [30] is used to simulate Bethe-Heitler events. To simulate the background sources (see section 3), diffractive ρ, ω and ϕ meson events are generated with the DIFFVM Monte Carlo [31], dilepton production through a photon-photon interaction is simulated using the GRAPE program [32].

3 Event Selection

The cross section of the Bethe-Heitler process, proceeding via Bremsstrahlung from the positron lines, is the largest when the positron and the photon are both produced in the backward direction. In the DVCS case, the final state photon does not originate from the positron and therefore the ratio of DVCS over BH process is expected to increase when the photon is found in the forward direction. The analysis is thus restricted to the case where the photon is detected in the central or in the forward parts of the detector, i.e. in the LAr calorimeter. A data sample, dominated by Bethe-Heitler events, is used as a reference sample to monitor the detector performance and its simulation. Two event samples are selected.

- **Enriched DVCS sample:** The photon candidate is detected in the LAr calorimeter and the positron candidate in the SpaCal calorimeter. Both DVCS and Bethe-Heitler processes are expected to contribute to this sample with similar magnitudes.
- **Control sample:** The photon candidate is detected in the SpaCal calorimeter and the positron candidate in the LAr calorimeter. The contribution of DVCS to this sample is negligible.

The event selection is based on the detection of exactly two electromagnetic clusters, corresponding to the final state photon and positron. One cluster is required to be detected in the SpaCal calorimeter with energy larger than $15\,\mathrm{GeV}$ and the other one in the LAr calorimeter ($25^\circ - 145^\circ$) with a transverse momentum $p_t > 1\,\mathrm{GeV}$. Events with more than one track are rejected. Events with one track are only kept if the track is associated to one of the clusters which hence identifies the positron candidate. If no track is reconstructed, the SpaCal cluster is assumed to be the positron. In order to reject inelastic and proton dissociation events, no further cluster in the LAr calorimeter with energy above $0.5\,\mathrm{GeV}$ is allowed and the absence of activity above the noise level in forward detectors PRT and FMD is required. The influence of

[2]The free parameters have been set in the simulation to the following values: the t-slope parameter $b = 7\,\mathrm{GeV}^{-2}$, the phase of the QCD amplitude, $\eta_{QCD} = 1 - \frac{\pi}{2}(0.176 + 0.33 \log Q^2)$ [28] and the sensitivity to the skewedness of the parton densities $R_\gamma = 0.55$ [16]. The proton structure function as extracted from the H1 data [29] has been used.

QED radiative corrections is reduced by requirements on the longitudinal momentum balance[3]. To enhance the DVCS signal with respect to the Bethe-Heitler contribution, and to maintain a large detector acceptance, the kinematic domain is explicitly restricted to: $2 < Q^2 < 20\,\mathrm{GeV}^2$, $|t| < 1\,\mathrm{GeV}^2$ and $30 < W < 120\,\mathrm{GeV}$. It has to be noted that for the BH process, the Q^2 and W variables cannot be associated with the photon virtuality and the $\gamma^* p$ center of mass energy, respectively.

3.1 Control sample

This sample of 338 events is dominated by the Bethe-Heitler process. Due to the large scattering angle of the positron, the DVCS process is suppressed to negligible levels. In order to have a control of the detector response in the same energy and angular ranges as for the enriched DVCS sample, the kinematic cuts in Q^2 and W are applied to this sample, treating the photon candidate in SpaCal as the scattered positron and the positron candidate in the LAr calorimeter as the photon. Background contributions from inelastic Bethe-Heitler events, diffractive ρ meson production and electron pair production have to be considered. The contribution of inelastic Bethe-Heitler events is estimated to be $7.7 \pm 3.8\,\%$. The diffractive electro production of ρ mesons constitutes a background when one of the decay pions is mis-identified as a positron in the calorimeter and the other pion is undetected, while the positron scattered into the SpaCal calorimeter is taken to be the photon. The elastic production of electron pairs by photon-photon processes $e^+p \to e^+e^-e^+p$ contributes to the background when only two of the three leptons are detected. These processes have been simulated using the Monte Carlo programs COMPTON 2.0 (both for elastic and inelastic BH), DIFFVM and GRAPE respectively. In the left column of Fig. 3, event distributions of the control sample are shown. The data are compared to the sum of the absolute MC predictions which includes the Bethe-Heitler process, elastic ρ production and elastic dilepton production, all normalised to luminosity. A good description of the data by the sum of the different MC samples is achieved, showing that the detector response is well described by the simulation.

3.2 Enriched DVCS sample

This sample (172 events) is found to be dominated by the DVCS contribution although the contribution of the Bethe-Heitler process is non negligible. An important contamination to DVCS elastic candidates is due to the DVCS process with proton dissociation:

$$e^+ + p \to e^+ + \gamma + Y, \tag{6}$$

when the decay products of the baryonic system Y are not detected in the forward detectors. The sum of non elastic DVCS and BH contributions has been estimated to be $16 \pm 8\,\%$ of the final sample [27], based on the fraction of events with proton dissociation tagged by the forward detectors and the detection efficiency of the forward detectors for proton dissociation events using the DIFFVM Monte Carlo. The other sources of background to be considered are due

[3]The quantity $\sum E - P_z$ is required to be above $45\,\mathrm{GeV}$. E denotes the energy and P_z is the momentum along the beam axis of the final state particles. The sum is calculated for the final state positron and photon.

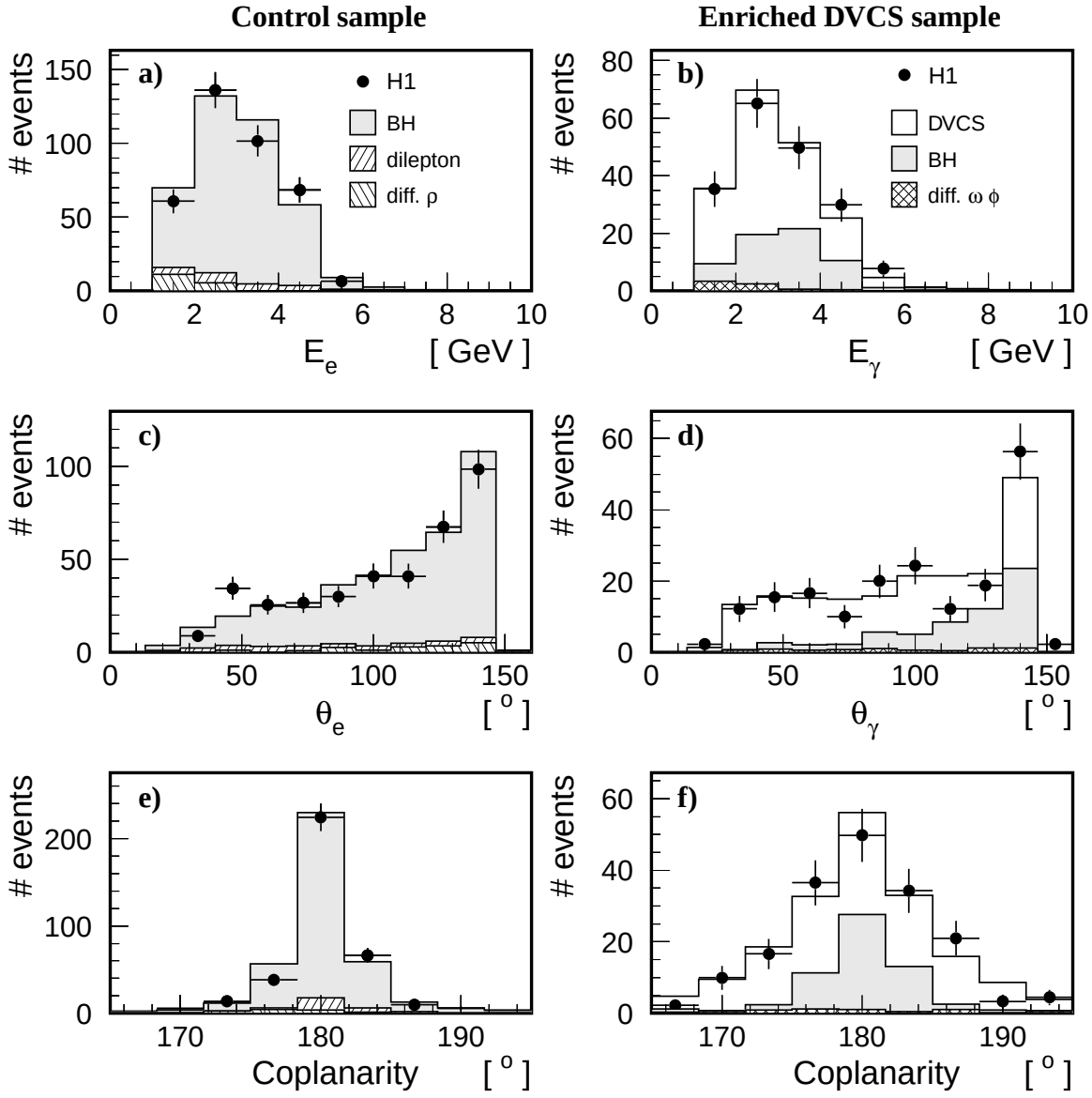

Figure 3: *Event distributions of the control sample (left) and of the enriched DVCS sample (right). a-b) energy of the cluster in the LAr calorimeter, c-d) polar angle of the cluster in the LAr calorimeter, e-f) coplanarity, i.e. difference of the azimuthal angle of the positron and photon candidates. The error bars on data points are statistical. Control sample: the cluster in the LAr calorimeter corresponds to the positron candidate. The data are compared to the sum of the predictions for the Bethe-Heitler process, elastic dilepton production and diffractive ρ production. All predictions are normalised to luminosity. Enriched DVCS sample: the cluster in the LAr calorimeter corresponds to the photon candidate. The data are compared to the sum of the predictions for the $e^+p \to e^+\gamma p$ reaction according to FFS, added to ω and ϕ diffractive backgrounds. The backgrounds and the BH contribution (shown on top of the backgrounds) are normalised to luminosity whereas the DVCS prediction is normalised in such a way that the sum of all contributions is equal to the total number of events.*

to diffractive ω and ϕ production, with decay modes to final states including photons (directly or from π^0 decay) or K^0_L. The main contributions originate from $\omega \to \pi^0\gamma$ and $\phi \to K^0_L K^0_S$ followed by $K^0_S \to \pi^0\pi^0$. The background arising from π^0 production, with the decay photons reconstructed in a single cluster, in low multiplicity DIS, is estimated from data. According to the MC simulation the two decay photons are recognised, in this energy range, in $20\,\%$ of the events in separate clusters. The selection has thus been extended to events with at least two clusters in the LAr calorimeter of energies exceeding $0.5\,\mathrm{GeV}$. The two photon invariant mass spectrum is in agreement with expectation from diffractive ω and ϕ production. Background from π^0 production is therefore inferred to be negligible. Figure 3 shows data distributions in comparison to the sum of the predictions according to the FFS calculation and the diffractive ω and ϕ backgrounds. The BH contribution in the FFS prediction and the ω and ϕ backgrounds are normalised to luminosity. The DVCS contribution in the FFS prediction is here normalised such that the sum of all contributions is equal to the total number of events in the data. The pure Bethe-Heitler contribution is also shown. The DVCS signal exhibits different kinematic distributions from the Bethe-Heitler contributions, in particular in the polar angle of the LAr cluster (Fig. 3c-d) and in coplanarity (Fig. 3e-f), which is defined as the difference of the azimuthal angles of the two clusters and is related to the p_t-balance of the positron-photon system. The coplanarity distribution is found to be broader ($\mathrm{rms} = 5.3°$) for the sum of the contribution in the enriched DVCS sample than for the Bethe-Heitler dominated control sample ($\mathrm{rms} = 3.2°$). This is attributed to the electromagnetic nature of the BH process which implies a steeper t distribution than the DVCS signal.

4 Cross section measurement and model comparison

To extract the cross section, the data of the enriched DVCS sample have been corrected for detector effects, acceptance and for initial state radiation of real photons from the positron line using the Monte Carlo simulation. The bin size has been chosen according to the statistical accuracy and is large with respect to resolutions in Q^2 ($12\,\%$) and W ($6\,\%$). The contamination of inelastic BH and DVCS events with proton dissociation ($16 \pm 8\,\%$) is subtracted statistically. The background contributions from diffractive ω and ϕ production, estimated to be $3.5\,\%$ on average and below $6\,\%$ in all bins, have been subtracted bin by bin.

The $e^+p \to e^+\gamma p$ cross section is presented in Fig. 4 and in Table 1 differentially in Q^2 and W. The data are compared to the estimate of the pure Bethe-Heitler contribution. The total cross section is dominated by the DVCS process at small W values and the Bethe-Heitler process at large W values. With the present precision, the Q^2 slopes of the two processes appear similar. The limited resolution and statistics do not allow the cross section measurement differentially in t and the extraction of the slope from the present data. The main contribution, of $8\,\%$, to the systematic error arises from detector effects and is due to the uncertainty on the measurement of the angle of the scattered positron. Other detector related errors are estimated to be around or below $2\,\%$. The second largest systematic error arises from the estimate of the contamination of non elastic BH and DVCS ($8\,\%$). The total systematic error is found to be around $15\,\%$.

In the leading twist approximation the contribution of the interference term to the cross

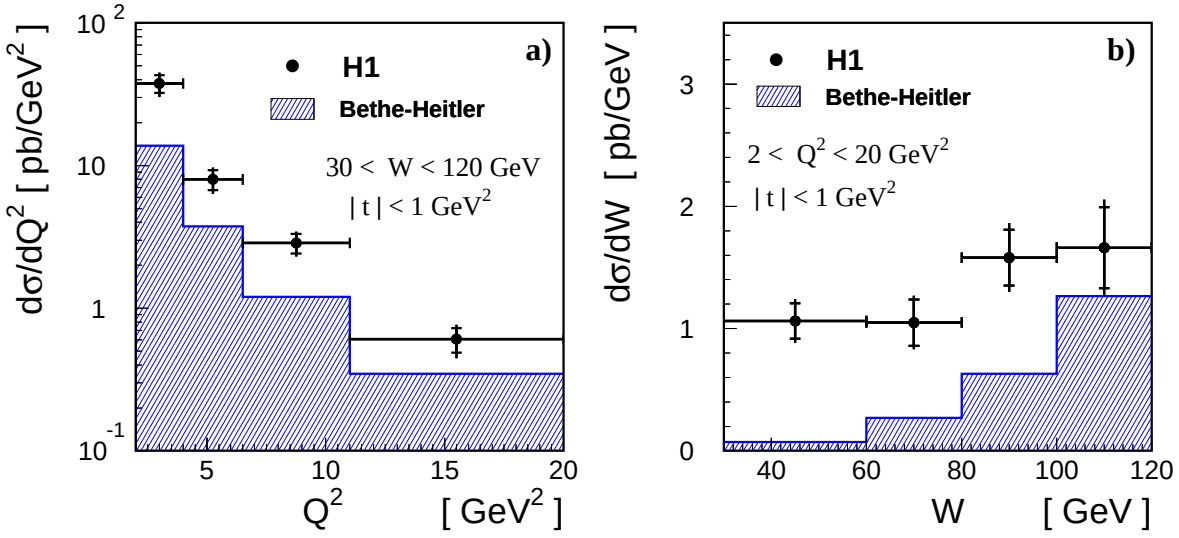

Figure 4: *Differential cross section measurements for the reaction $e^+p \to e^+\gamma p$ as a function of Q^2 (a) and W (b). The inner error bars are statistical and the full error bars include the systematic errors added in quadrature. The hatched histogram shows the contribution of the Bethe-Heitler process to the reaction, where, however, Q^2 and W do not correspond to the photon virtuality and the γ^*p center of mass energy, respectively.*

section is proportional to the cosine of the photon azimuthal angle[4]. Since the present measurement is integrated over this angle, the overall contribution of the interference term is negligible. Therefore the Bethe-Heitler cross section can be subtracted from the total cross section in order to obtain the DVCS cross section. The DVCS $e^+p \to e^+\gamma p$ cross section is then converted to a DVCS $\gamma^*p \to \gamma p$ cross section using the equivalent photon approximation (as in [11]).

Q^2 $[\mathrm{GeV}^2]$	$d\sigma^{e^+p\to e^+p\gamma}/dQ^2$ $[\mathrm{pb}/\mathrm{GeV}^2]$		
$[2.0, 4.0]$	37.6	± 5.3	± 5.1
$[4.0, 6.5]$	8.0	± 1.3	± 1.1
$[6.5, 11.0]$	2.87	± 0.46	± 0.35
$[11.0, 20.0]$	0.61	± 0.12	± 0.11

W [GeV]	$d\sigma^{e^+p\to e^+p\gamma}/dW$ [pb/GeV]		
$[30, 60]$	1.06	± 0.15	± 0.10
$[60, 80]$	1.05	± 0.19	± 0.11
$[80, 100]$	1.58	± 0.23	± 0.16
$[100, 120]$	1.66	± 0.33	± 0.21

Table 1: *Differential cross sections for the reaction: $e^+p \to e^+p\gamma$, as a function of Q^2 and W, in the kinematic domain $2 < Q^2 < 20\,\mathrm{GeV}^2$, $30 < W < 120\,\mathrm{GeV}$ and $|t| < 1\,\mathrm{GeV}^2$. The first errors are statistical, the second systematic.*

The γ^*p cross section for the DVCS process is shown in Fig. 5 and given in Table 2 as a function of Q^2 for $W = 75\,\mathrm{GeV}$, and as a function of W for $Q^2 = 4.5\,\mathrm{GeV}^2$. The systematic errors on the γ^*p cross section are due to the propagation of the systematic errors on the e^+p cross section combined with the bin center corrections error (7 %). The data are compared with the predictions by FFS and DD. The shape of the data is well described by both calculations both in Q^2 and W. The absence of predictions for the t-slope leaves an uncertainty on the

[4]The photon azimuthal angle is defined as the angle between the plane formed by the incoming and scattered positrons and the γ^* proton plane.

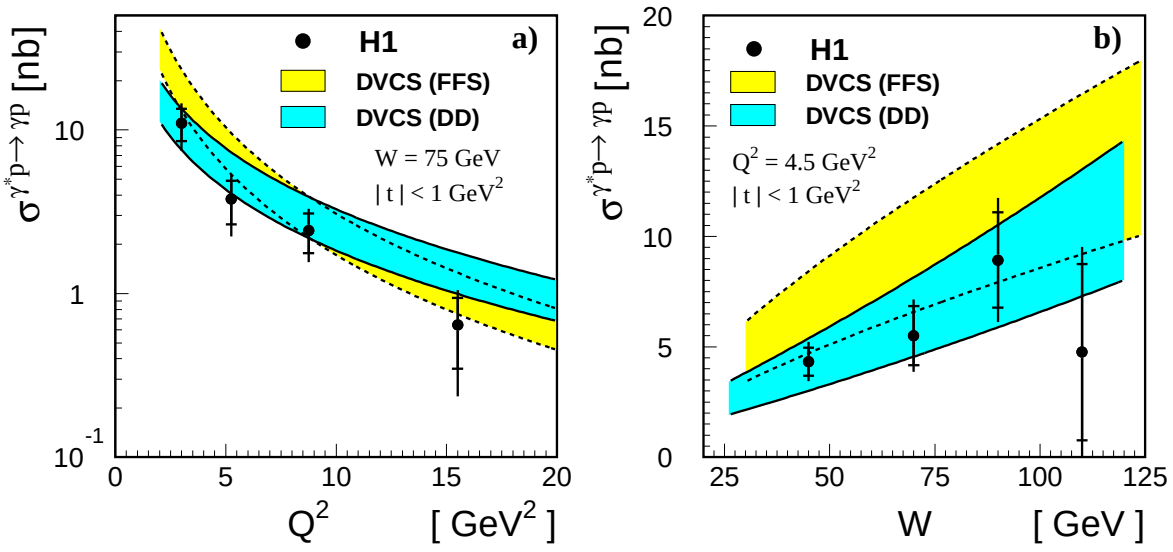

Figure 5: *Cross section measurements for the $\gamma^* p \to \gamma p$ DVCS process as a function of Q^2 (a) and W (b). The data are compared to the theoretical predictions of FFS* [16] *and DD* [17]*. The band associated to each prediction corresponds to a variation of the assumed t-slope from $5\ \mathrm{GeV}^{-2}$ (upper bound) to $9\ \mathrm{GeV}^{-2}$ (lower bound). The inner error bars are statistical and the full error bars include the systematic errors added in quadrature.*

normalisation of the theoretical models. The band associated to each prediction corresponds to a variation of the t-slope of $5 < b < 9\ \mathrm{GeV}^{-2}$, covering the measured range for light vector meson production [11,14]. Both predictions are consistent with the data within this uncertainty. It is noted that these data provide constraints also for recent NLO calculations, which invoke skewed parton distributions [33].

Q^2 $[\mathrm{GeV}^2]$	$\sigma^{\gamma^* p \to \gamma p}$ [nb]		
3.0	11.0	± 2.4	± 2.5
5.25	3.8	± 1.1	± 1.0
8.75	2.43	± 0.66	± 0.54
15.50	0.64	± 0.30	± 0.28

W [GeV]	$\sigma^{\gamma^* p \to \gamma p}$ [nb]		
45	4.33	± 0.64	± 0.54
70	5.51	± 1.34	± 0.86
90	8.9	± 2.2	± 1.7
110	4.8	± 4.0	± 2.6

Table 2: *Measured cross section for the elastic DVCS process $\gamma^* p \to \gamma p$ as a function of Q^2 for $W = 75\,\mathrm{GeV}$ and as a function of W for $Q^2 = 4.5\,\mathrm{GeV}^2$, both for $|t| < 1\,\mathrm{GeV}^2$. The first errors are statistical, the second systematic.*

5 Conclusion

The DVCS process has been studied in the kinematic region $2 < Q^2 < 20\,\mathrm{GeV}^2$, $30 < W < 120\,\mathrm{GeV}$ and $|t| < 1\,\mathrm{GeV}^2$ using a data sample taken by the H1 detector and corresponding to an integrated luminosity of $8\,\mathrm{pb}^{-1}$. The cross section for the reaction $e^+ p \to e^+ \gamma p$ has been measured for the first time and presented differentially in Q^2 and W. The DVCS process is

observed to dominate over the Bethe-Heitler process for $W \lesssim 100$ GeV. The $\gamma^* p$ DVCS cross section has been extracted and compared to the QCD based predictions [16, 17] which both describe the measured Q^2 and W distributions within errors.

Acknowledgements

We are grateful to the HERA machine group whose outstanding efforts have made and continue to make this experiment possible. We thank the engineers and technicians for their work in constructing and now maintaining the H1 detector, our funding agencies for financial support, the DESY technical staff for continual assistance and the DESY directorate for the hospitality which they extend to the non DESY members of the collaboration. We are grateful to M. Diehl and A. Freund for valuable discussions.

References

[1] X. Ji, Phys. Rev. **D 55** (1997) 7114 [hep-ph/9609381].

[2] J. C. Collins and A. Freund, Phys. Rev. **D 59** (1999) 074009 [hep-ph/9801262].

[3] X. Ji and J. Osborne, Phys. Rev. **D 58** (1998) 094018 [hep-ph/9801260].

[4] J. Blümlein and D. Robaschik, Nucl. Phys. **B581** (2000) 449 [hep-ph/0002071].

[5] L. Mankiewicz, G. Piller, E. Stein, M. Vanttinen and T. Weigl, Phys. Lett. **B425** (1998) 186 [hep-ph/9712251].

[6] A. V. Belitsky, D. Müller, L. Niedermeier and A. Schäfer, Phys. Lett. **B474** (2000) 163 [hep-ph/9908337].

[7] D. Müller, D. Robaschik, B. Geyer, F. M. Dittes and J. Hořejši, Fortsch. Phys. **42** (1994) 101 [hep-ph/9812448].

[8] X. Ji, Phys. Rev. Lett. **78** (1997) 610 [hep-ph/9603249].

[9] A. V. Radyushkin, Phys. Rev. **D 56** (1997) 5524 [hep-ph/9704207].

[10] A. Airapetian [HERMES Collaboration], DESY 01-091 and hep-ex/0106068, submitted to Phys. Rev. Lett.

[11] S. Aid *et al.* [H1 Collaboration], Nucl. Phys. B **468** (1996) 3 [hep-ex/9602007], C. Adloff *et al.* [H1 Collaboration], Eur. Phys. J. C **13** (2000) 371 [hep-ex/9902019].

[12] J. Breitweg *et al.* [ZEUS Collaboration], Eur. Phys. J. C **6** (1999) 603 [hep-ex/9808020].

[13] C. Adloff *et al.* [H1 Collaboration], Eur. Phys. J. C **10** (1999) 373 [hep-ex/9903008].

[14] C. Adloff *et al.* [H1 Collaboration], Phys. Lett. B **483** (2000) 360 [hep-ex/0005010].

[15] M. Derrick *et al.* [ZEUS Collaboration], Phys. Lett. B **380** (1996) 220 [hep-ex/9604008].

[16] L. L. Frankfurt, A. Freund and M. Strikman, Phys. Rev. **D 58** (1998) 114001 and *erratum* Phys. Rev. **D 59** 1999 119901E [hep-ph/9710356].

[17] A. Donnachie and H. G. Dosch, Phys. Lett. B **502** (2001) 74 [hep-ph/0010227].

[18] J. D. Bjorken and J. B. Kogut, Phys. Rev. D **8** (1973) 1341.

[19] C. Adloff *et al.* [H1 Collaboration], Phys. Lett. B **483** (2000) 23 [hep-ex/0003020].

[20] J. Breitweg *et al.* [ZEUS Collaboration], Phys. Lett. B **437** (1998) 432 [hep-ex/9807020].

[21] M. Diehl, T. Gousset, B. Pire and J. P. Ralston, Phys. Lett. **B411** (1997) 193 [hep-ph/9706344].

[22] A. Freund, Phys. Lett. **B472** (2000) 412 [hep-ph/9903488].

[23] A. V. Belitsky, D. Müller, L. Niedermeier and A. Schäfer, Nucl. Phys. B **593** (2001) 289 [hep-ph/0004059].

[24] I. Abt *et al.* [H1 Collaboration], Nucl. Instrum. Meth. A **386** (1997) 310 and 348.

[25] R. D. Appuhn *et al.* [H1 SPACAL Group Collaboration], Nucl. Instrum. Meth. A **386** (1997) 397.

[26] B. Andrieu *et al.* [H1 Calorimeter Group Collaboration], Nucl. Instrum. Meth. A **350** (1994) 57.

[27] R. Stamen, PhD dissertation, Universität Dortmund and Université Libre de Bruxelles, in preparation, made available through: http://www-h1.desy.de/publications/theses_list.html

[28] H. Abramowicz and A. Levy, DESY 97-251, [hep-ph/9712415].

[29] C. Adloff *et al.* [H1 Collaboration], DESY-00-181, hep-ex/0012053, accepted by Eur. Phys. J. C.

[30] A. Courau, S. Kermiche, T. Carli and P. Kessler, *Quasi-Real QED Compton Monte Carlo, Proceedings of the Workshop on Physics at HERA,* Vol. 2: 902-915, Hamburg 1991.

[31] B. List, A. Mastroberardino, *DIFFVM: A Monte Carlo generator for diffractive processes in ep scattering, Proceedings of the Monte Carlo Generators for HERA physics*, DESY-PROC-1999-02, p. 396.

[32] T. Abe et al., *GRAPE-Dilepton, Proceedings of the Monte Carlo Generators for HERA physics*, DESY-PROC-1999-02, p. 566.

[33] A. Freund and M. F. McDermott, hep-ph/0106124.